J. Indian Chem. Soc.,
Vol. 97, No. 11a, November 2020, pp. 2155-2165

Syntheses of hematite and maghemite nanocrystals from a single metal-organic precursor for catalytic use

Ruhul A. Bepari[a,b], Anamika Talukdar[c], Monideepa Chakrabortty[c], Zinnatara Islam[b] and Birinchi K. Das*[b,d]

[a]Department of Chemistry, B. N. College, Dhubri-783 324, Assam, India

[b]Department of Chemistry, Gauhati University, Guwahati-781 014, Assam, India

[c]Department of Chemistry, Assam Engineering College, Guwahati-781 013, Assam, India

[d]Bhattadev University, Bajali, Pathsala-781 325, Assam, India

E-mail: birinchi.das@gmail.com

Manuscript received online 14 October 2020, revised and accepted 31 November 2020

Iron(II) isonicotinate tetrahydrate has been used as the metal-organic precursor for the synthesis of the α and γ phases of nanocrystalline Fe_2O_3. Solvothermal aging of an alkaline ethanolic solution of the precursor at 120°C gives α-Fe_2O_3 (hematite) nanorods, while spherical γ-Fe_2O_3 (maghemite) nanoparticles are obtained from its alkaline ethylene glycolic solution at 180°C. Smaller maghemite nanoparticles have been prepared via poly(vinylpyrrolidone) (PVP) coating. Both forms of iron oxide materials have been characterized by XRD, TEM, and Raman, IR and UV-Vis spectroscopy. Single crystalline α-Fe_2O_3 nanorods of ~12 nm diameter are obtained at low precursor concentrations. The α-Fe_2O_3 materials are superparamagnetic while uncoated γ-Fe_2O_3 and PVP-coated γ-Fe_2O_3 samples are ferromagnetic and superparamagnetic respectively. Preliminary studies show that these iron oxides are active as magnetic nanocatalysts in the selective epoxidation of styrene with aqueous *tert*-butylhydroperoxide as the oxidant.

Keywords: Precursor method, hematite, maghemite, magnetic nanocatalyst, styrene epoxidation.

Introduction

The metal(II) isonicotinate tetrahydrates for M = Mn, Fe, Co, Ni, Cu and Zn constitute a compositionally stable series of simple metal complexes which can be easily isolated in high yield at room temperature[1]. Their structures have been analyzed with single crystal and powder X-ray diffraction[2] as well as XAFS[3] methods, while their isostructurality[2], spectral[1] and thermal behavior[4] and suitability as precursor species for the synthesis of metal oxides such as NiO[5] and ZnO[6] have also been studied. Iron(II) isonicotinate is isolable as an air-stable canary yellow product that may be thermally converted to its oxide like those of the corresponding nickel and zinc species[4]. α- and γ-Fe_2O_3, Fe_3O_4 nanoparticles were obtained earlier via thermal decomposition of tris(acetylacetonato)iron(III) at a lower temperature in air[7]. Preparation of monodispersed γ-Fe_2O_3 nanocrystals employing ferrocene as the precursor was also reported in the literature[8]. Zhao *et al.* reported a novel method of producing maghemite nanopowder via thermal decomposition of an Fe(III)-urea complex[9].

Although work on the synthesis of nanoscale iron oxides using iron complexes as precursors has been published earlier, most of the reported methods suffer from the drawbacks of long reaction time, high reaction temperature, inhomogeneous size distribution and poor crystallinity of the resultant oxide materials. Thus, the reproducible preparation of iron oxide nanoparticles with desired morphologies under mild condition appeared to us as a challenging problem to be addressed. In the present study, we have developed an efficient template-free solvothermal method for the synthesis of hematite nanorods under mild condition using iron(II) isonicotinate tetrahydrate, i.e. the *trans*-[$Fe(NC_5H_4$-*p*-$CO_2)_2(OH_2)_4$] complex as the precursor. On the other hand, low temperature thermolysis of the same metal-organic species carried out both in the absence and in presence of

poly(vinylpyrrolidone) (PVP) has been found to yield maghemite nanoparticles.

Since oxides of iron have been shown previously[10–13] to be effective as heterogeneous catalysts in the oxidation of styrene, we have tested the nanostructured α- and γ-Fe_2O_3 synthesized by us for the same reaction by making use of *tert*-tetrabutylhydroperoxide (TBHP) as the terminal oxidant.

Experimental

Materials and methods:

Isonicotinic acid, PVP (M_w = 29,000), styrene, and TBHP were purchased from Sigma-Aldrich. Common chemicals were procured from E. Merck (India). All the chemicals were used without further purification. Ferrous isonicotinatetetrahydrate, i.e. *trans*-[$Fe(NC_5H_4$-*p*-$CO_2)_2(OH_2)_4$], was prepared by following the procedure developed earlier in this laboratory[1].

X-Ray powder diffraction patterns of the synthesized oxide samples were recorded on a Philips X'pert Pro X-ray diffractometer with Cu-Kα radiation (λ = 1.5418 Å) with 2θ ranging from 15 to 80°. Transmission electron microscopic (TEM) images were recorded on two different high resolution electron microscopes: HRTEM-JEOL, model 1200 EX operating at 100 kV and TEM-JEOL JEM-2100 operating at 200 kV. A Hitachi U-4200 spectrophotometer was used to obtain diffuse reflectance spectra (DRS) from dried powdery films mounted on glass slide using $BaSO_4$ for preparing the film. IR spectra were recorded using a Shimadzu IR Affinity-1 instrument in the 4000–400 cm^{-1} range for KBr pellets. FT-Raman spectra were recorded on a Horiba Jobin-Yvon Lab RAMHR High Resolution Raman Spectrometer using green light (514 nm) for excitation. Measurements were performed at room temperature with laser power of 20 mW (on the samples). Magnetic measurements were performed at room temperature using either a Lakeshore 7410 or PAR EG & G 4500 vibrating sample magnetometer (VSM). Gas chromatography (GC) for catalytic studies was done on a Varian-450 GC equipped with flame ionization detector (FID) fitted with a CP-Sil 8 CB capillary column (5 μm coated with cross-linked methyl silicone gum, 0.2 mm×50 m).

Synthesis of hematite nanorods:

In a typical procedure, 300 mg of NaOH was dissolved in 50 mL of ethanol under mechanical stirring. The reaction solution immediately turned blood red upon the addition of 1 g of ferrous isonicotinate tetrahydrate to it. After 15 min of vigorous stirring at room temperature, the reaction mixture was transferred into a 100 mL teflon-lined stainless steel autoclave which was then put in an oven heated at 120°C and aged for 4 h. Then, it was allowed to cool down to room temperature naturally. The red oxide powder was collected by means of centrifugation and washed several times with de-ionized (DI) water and finally once with ethanol. The product was dried at 60°C for 6 h. Yield: 0.21 g (~94%).

Several time-dependent syntheses were also carried out where the reaction mixture was subjected to autoclaving for different times (2–20 h) with a fixed precursor concentration. Additionally, solvothermal treatments were also carried out with varying precursor concentrations (0.5–1 g) for same periods of time.

Synthesis of maghemite nanoparticles:

In a typical synthesis, 500 mg of NaOH was dissolved in 75 mL of ethylene glycol and to this 1.5 g of ferrous isonicotinate tetrahydrate was added. The reaction mixture was stirred at 180°C (oil bath temperature) for 10 min. The reaction mixture turned blood red upon the addition of the iron complex which appeared to change rapidly into green initially. In the subsequent step, 3 g of anhydrous sodium acetate (NaOAc) was added to the reaction mixture and the stirring was continued further for 30 min at the same temperature (180°C). As the reaction proceeded (15–20 min), color of the reaction mixture started changing slowly to red-brown indicating the formation of maghemite particles. It was then allowed to cool down to room temperature. The maghemite nanoparticles were harvested by means of an external magnet, washed several times with DI water and finally dried at 60°C for 6 h. Yield: 0.31 g (~96%).

For the synthesis of PVP coated γ-Fe_2O_3 nanoparticles, the above procedure of thermal decomposition of ferrous isonicotinate was repeated. After dissolving the required amount (500 mg) of NaOH in ethylene glycol (75 mL), 1.5 g of PVP was added to the reaction mixture and the procedure described above for the synthesis of uncoated γ-Fe_2O_3 was followed thereafter.

Catalytic studies:

A typical oxidation reaction was performed in a round-bottomed flask fitted with a water-cooled condenser using 70% aqueous TBHP as the oxidant. To the mixture of sub-

strate (5 mmol), TBHP (2 mL, 14 mmol) and acetonitrile (5 mL), the iron oxide catalyst (10 mg) was added and the flask containing the stirred reaction mixture was heated at a constant temperature of 70°C on an oil bath. The progress of the reaction was monitored by making use of GC. Samples of the reaction mixture were withdrawn at regular time intervals and in each case the catalyst was filtered off or removed by centrifugation prior to GC examination. Products were identified by comparing them with authentic samples and further confirmed by GC-MS (Shimadzu 2000A), while substrate conversion as well as product yields were determined by GC.

Results and discussion

Synthesis:

We have adopted the precursor compound method[14] to synthesize iron(III) oxide nanomaterials by making use of a well-defined iron(II) complex viz. *trans*-[Fe(NC_5H_4-*p*-CO_2)$_2$(OH_2)$_4$] which may be alternatively called ferrous isonicotinate tetrahydrate. This canary yellow species may be reproducibly synthesized in excellent yield at room temperature[1]. While the precursor complex was dissolved in alkaline ethanol to obtain nanorods of α-Fe_2O_3 at the end of a four-hour solvothermal reaction at 120°C, replacement of ethanol with ethylene glycol gave the right conditions to obtain spherical nanoparticles of γ-Fe_2O_3 under atmospheric pressure and in presence of added sodium acetate at 180°C. Presence of PVP during the latter synthesis enabled us to achieve enhanced dispersion and smaller particles of the intended maghemite species. In all cases the isolated yields of the nanomaterials were found to be excellent.

In order to understand the growth mechanism of α-Fe_2O_3 nanorod formation we carried out several synthetic reactions by focusing our attention on how the length of solvothermal aging and precursor concentration could influence the size, morphology and crystallinity of the hematite particles. Appearance of red coloration upon addition of the precursor complex to alkaline ethanol containing ~5% water suggests the instantaneous formation of an iron(III) species which grows further in an oriented manner during the solvothermal aging. Similar growth of hematite nanoparticles was earlier observed by Chen *et al.* using ethanol as solvent[15]. Literature also reveals that the carboxyl group (RCOOH, R = CH_3, C_2H_5, C_6H_5 etc.) has a coordinative influence on the formation of 1-D nanostructures[16]. Therefore, a partial contribution of the isonicotinato ligand [NC_5H_4-*p*-COO^-], present in the iron precursor itself, is likely to be important in the formation of the observed rod-like structures of the α-Fe_2O_3 product obtained by us.

The solvothermal approach developed by us has several advantages over the existing procedures. These include short autoclaving time (1–4 h), low reaction temperature (120°C), highly crystalline products and excellent control over the particle size and morphology. It is possible to obtain hematite nanoparticles even after 1 h solvothermal aging of the starting reaction mixture. Although, the oxide particles are non-crystalline at this stage of the solvothermal treatment, the crystallinity grows rapidly with time (2 h). Furthermore, the present method provides an easy way to synthesize α-Fe_2O_3 with rod-like morphology without using any additive or template. The excellent product yield (94%) further reflects the usefulness of this preparative route. Additionally, the air-stable iron(II) precursor used in this synthesis can also be prepared in a facile manner. Our finding also has clear advantages over situations where synthesis of hematite nano rods required calcination following solvothermal aging[17], use of very high decomposition temperatures[18], surfactants as templates[19] and long reaction time[18].

It has been observed that reaction temperature plays an important role in the thermal decomposition of the precursor complex in the present instance. Thus, when the decomposition was carried out at lower temperatures (< 180°C), no maghemite particle was found to form. Furthermore, when the synthesis was performed without NaOAc, which is known[20] to be a useful precipitating agent, no maghemite particle formed. The thermal decomposition of iron complexes have traditionally been carried out at higher temperatures under inert atmosphere to fabricate iron oxide nanoparticles with desired phase identity, composition and crystallinity. For example, an iron-oleate species was decomposed at 300°C to prepare crystalline γ-Fe_2O_3 nanocrystals[21]. Maghemite-hematite core-shell structures were synthesized via thermolysis of an iron(III) complex at a temperature of 450°C for 3 h[22]. Relatively more expensive iron precursors like ferrocene were also used to obtain the oxide via thermolysis[8]. Clearly, the use of a low temperature (180°C), short decomposition time (30 min), atmospheric condition and an inexpensive precursor makes the present procedure more attractive over the existing thermolysis-based methods for the synthesis of γ-Fe_2O_3 nanocrystals.

Characterization:

Powder XRD technique was used for the phase identification of the synthesized materials. Then, detailed characterization was done with the help of various physical techniques.

X-Ray diffraction (XRD):

All the reflections in the X-ray diffractogram of the oxide product obtained via 20 h autoclaving (Fig. 1(a)) can be unambiguously indexed to pure hexagonal α-Fe_2O_3 with lattice constants *a* = 5.014 Å and *c* = 13.673 Å (JCPDS, Ref. 84-308). Then, diffractograms of the other samples have been compared with it. It is evident from the XRD patterns (Fig. 1) that peak intensity of the synthesized iron oxide materials increases gradually with increasing lengths of solvothermal aging used during synthesis. Thus, intense and sharp peaks observed in the diffractogram of the oxide sample obtained after 20 h aging suggests a high degree of crystallinity of the material. On the other hand, diffractograms of both the materials (Fig. 1(c, d)) obtained after 1 and 2 h solvothermal aging reflect their poor crystallinity. The diffractogram of the latter product displays five reflections at 2θ values of 33.3, 35.9, 49.7, 54.3, 63 and 64.1° which can be readily indexed to the (104), (110), (024), (116), (214) and (300) reflection planes of α-Fe_2O_3 respectively. Similarly, the diffractogram of the 1 h autoclaved product shows only three peaks at the 2θ values of 23.9, 35.8 and 63.7° for the hematite phase. The diffractogram of the oxide sample obtained after 4 h aging (Fig. 1(c)) shows an intermediate level of crystallinity of the material.

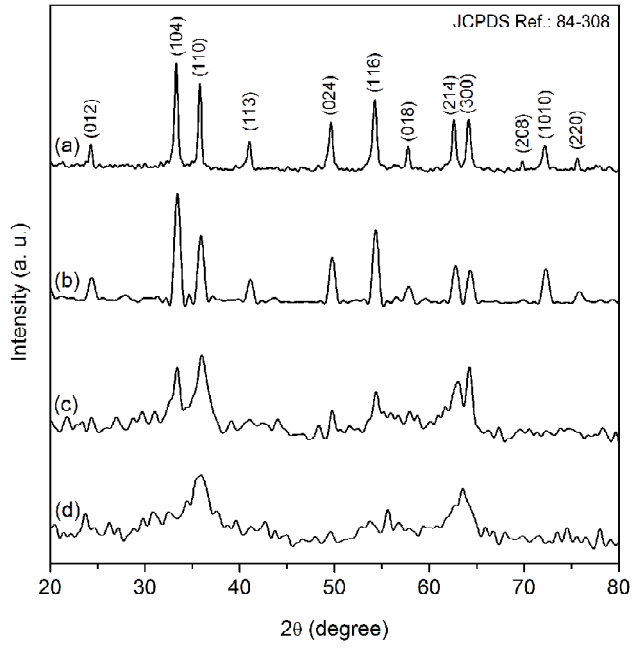

Fig. 1. XRD patterns of the α-Fe_2O_3 samples obtained after (a) 20 h, (b) 4 h, (c) 2 h and (d) 1 h solvothermal aging of 1 g of the ferrous isonicotinate tetrahydrate.

The powder XRD technique does not provide conclusive evidence to distinguish between the Fe_3O_4 and γ-Fe_2O_3 phases of iron oxide because structures of both the magnetic oxides are of the inverse spinel-type[23]. All the reflections in the diffractogram of uncoated maghemite sample (Fig. 2(a)) can be indexed to pure tetragonal γ-Fe_2O_3 with lattice constants *a* = 8.34 Å and *c* = 25.02 Å (JCPDS, Ref. 25-1402). The diffractogram of the uncoated γ-Fe_2O_3 is nearly identical with that of the PVP coated γ-Fe_2O_3. Therefore, both the samples can be interpreted as being γ-Fe_2O_3. Further phase analysis has been done by Raman spectroscopy (please see below).

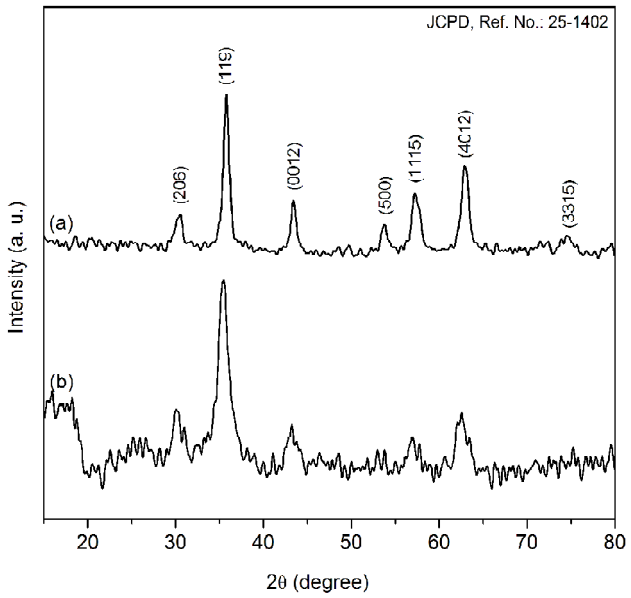

Fig. 2. XRD patterns of the (a) uncoated γ-Fe_2O_3 and (b) PVP coated γ-Fe_2O_3 nanoparticles.

Transmission electron microscopy (TEM):

The TEM image of the oxide sample produced after 4 h aging is presented in Fig. 3. It shows the rod-like morphology of the α-Fe_2O_3 particles with diameters of 5–7 nm and length about 80 nm. HRTEM image of a single nanorod suggests its structural uniformity with a lattice spacing of 2.23 Å

which fits the interplanar spacing of the (113) plane of hexagonal α-Fe_2O_3. SAED pattern can be assigned to the (012), (104), (113) and (300) planes of α-Fe_2O_3 with measured spacings of 3.45, 2.67, 2.50 and 1.42 Å respectively. Vis-à-vis the above result it is pertinent to add here that while no clearly defined particles can be seen in the TEM image of the iron oxide sample isolated at the end of 1 h autoclaving, poorly defined rod-like nanocrystals can be seen in the TEM image of the product obtained at the end of 2 h autoclaving. However, in the HRTEM images of these two materials lattice fringes characteristic of the α-Fe_2O_3 phase can be identified. Thus, TEM results suggest that complete growth of the hematite particles with rod-like morphology requires at least 4 h solvothermal treatment of the reaction mixture.

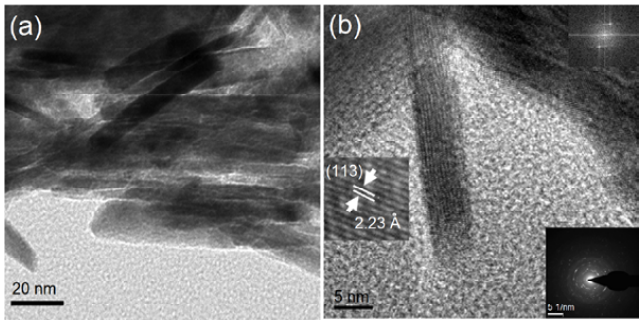

Fig. 3. (a) TEM and (b) HRTEM images of the α-Fe_2O_3 sample obtained after 4 h solvothermal aging. Insets of (b) show the lattice spacing with the corresponding FFT pattern and the SAED pattern.

In contrast with the above results, the TEM image of the oxide product prepared via 20 h autoclaving demonstrates ellipsoidal morphology with a mean diameter of 20 nm. Prolonged solvothermal aging may be responsible for the observed collapse of rod-like morphology of the oxide particles. These findings are consistent with earlier studies suggesting that solvothermal reaction time is one of the key factors that largely influences the particle size and morphology of oxide nanoparticles[17,24].

When the synthetic reaction was carried out for 2 h with reduced precursor concentration (0.5 g), keeping all other parameters constant, rod-like morphology of the oxide particles once again becomes clearer. Crystallinity of the nanorods also improves significantly. As per TEM results obtained by us, the rod-like α-Fe_2O_3 particles display ~12 nm diameter and they are of up to 250 nm length. Distinct lattice fringes (HRTEM image) reflect good crystalline nature of the nanorods. The measured spacing of 2.44 Å corresponds to the (110) plane of α-Fe_2O_3. Furthermore, the SAED pattern obtained from a single rod suggests the single-crystalline nature of the nanostructured oxide material obtained by us. Increased aging (4 h) of the reaction mixture under identical condition leads to an increase in length of the nanorods. Thus, TEM image shows the α-Fe_2O_3 nanorods with diameter of 7 nm and length up to 400 nm. Further increase in autoclaving time to 8 h shows no significant change in the size and morphology of the nanorods. Thus, TEM images (Fig. 4) show the α-Fe_2O_3 nanorods with average diameter of ~10 nm and length of about 100 nm. It is worth noting that the size distribution of the nanorods is homogenous. Distinct lattice fringes (HRTEM image) and well defined SAED pattern provide additional evidences for the high crystallinity of the nanorods. The interplanar spacing was found to be 2.55 Å which corresponds to the (110) plane of α-Fe_2O_3.

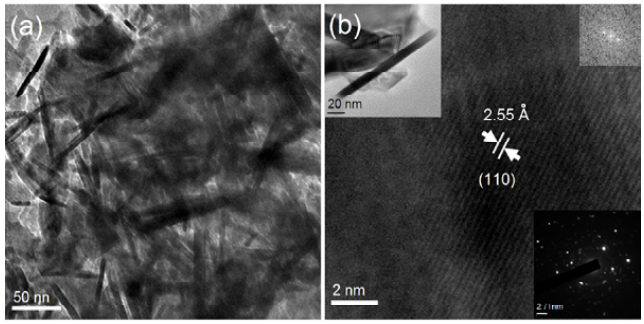

Fig. 4. (a) TEM and (b) HRTEM images of the α-Fe_2O_3 sample obtained after 8 h solvothermal aging. Insets of (b) show a single nanorod, lattice spacing with the corresponding FFT pattern and the SAED pattern.

TEM was also used to investigate the structural parameters of maghemite samples. Thus, the TEM image presented in Fig. 5 shows the largely agglomerated particles but HRTEM image still shows some spherical particles (encircled) with diameters ranging from 8–11 nm. The TEM image of the PVP coated γ-Fe_2O_3 (Fig. 6) shows nearly spherical particles with an average diameter of 5 nm. Agglomeration of the smaller particles into bigger ones is less effective in the presence of PVP. Adsorption of PVP macromolecules on the surface of magnetic nanocrystals is believed to retard the growth of oxide nanoparticles[25].

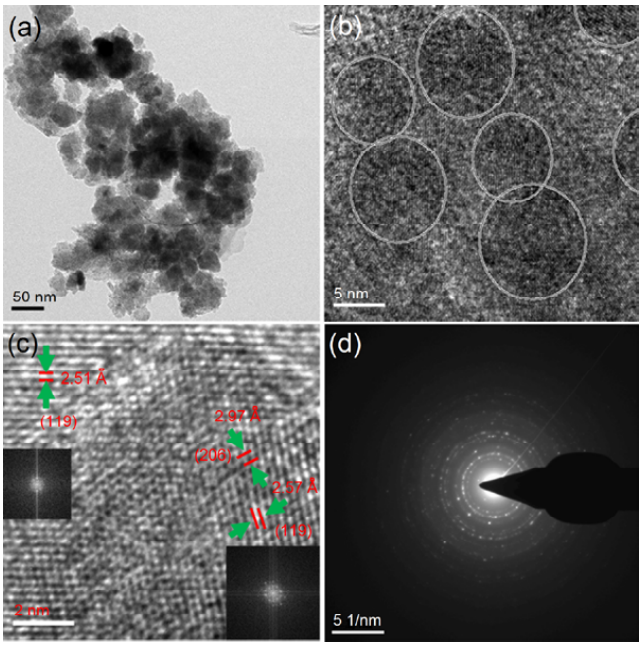

Fig. 5. (a) TEM, (b, c) HRTEM images and (d) SAED pattern of the as-synthesized γ-Fe_2O_3 sample. Insets of (c) show the lattice spacings with the corresponding FFT patterns.

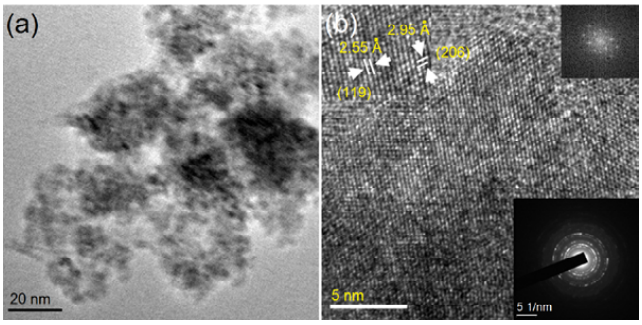

Fig. 6. (a) TEM, (b) HRTEM images of the as-synthesized PVP coated γ-Fe_2O_3 sample. Inset of (b) show the lattice spacing with the corresponding FFT pattern and the SAED pattern.

Raman spectroscopy:

Raman spectra of all the Fe_2O_3 materials synthesized at different solvothermal autoclaving times are presented in Fig. 7. Five strong resonance peaks located at 221, 287, 403, 493, and 601 cm^{-1} can be observed for each sample. The positions of the peaks are consistent with the typical frequencies observed for Fe_2O_3 and can be assigned to the $2A_{1g}$ and $3E_g$ vibrations[26]. The extra peak appearing in Fig. 7(b) indicates the presence of the magnetite phase[26]. Intensities of the Raman peaks (Fig. 7(a)) are quite low for the oxide material obtained after 1 h solvothermal aging. Literature suggests that in amorphous materials, relaxation of the Raman selection rules often arise due to the lack of long-range order and also due to the presence of disorder[26,27]. These two effects can trigger the broadening of Raman lines with decreasing crystal size, due to phonon confinement. The peak intensities gradually increase with increasing autoclaving of the samples (with increasing crystallinity). This observation is in good agreement with that of the XRD investigation.

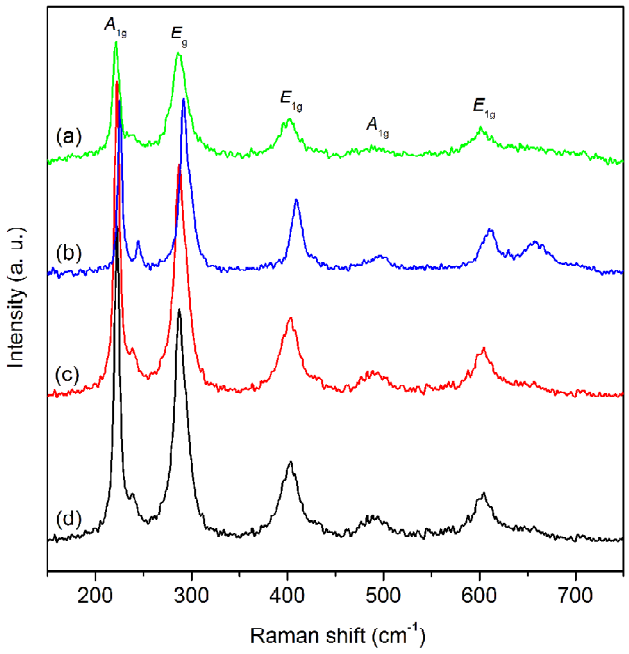

Fig. 7. Raman spectra of the α-Fe_2O_3 samples obtained after (a) 1 h, (b) 2 h, (c) 4 h and (d) 20 h solvothermal aging of 1 g of ferrous isonicotinate tetrahydrate.

Raman spectroscopy thus provides a method to differentiate the various phases of iron oxide[28]. Raman spectra (Fig. 8) of the iron oxide samples synthesized following the thermolysis route display five peaks located at 226, 293, 409, 497 and 610 cm^{-1} which can be assigned to α-Fe_2O_3[26]. It is noteworthy that the characteristic bands of magnetite at 668 and 535 cm^{-1} cannot be observed in the Raman spectra confirming the absence of the Fe_3O_4 phase[28,29]. During spectral measurement, laser irradiation usually leads to significant heat generation within the sample which alters the pro-

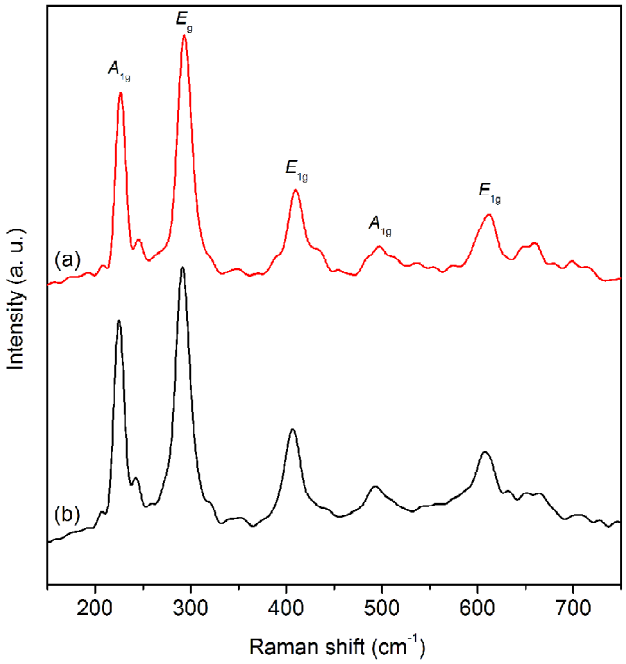

Fig. 8. Raman spectra of the as-synthesized (a) γ-Fe_2O_3 and (b) PVP coated γ-Fe_2O_3 samples.

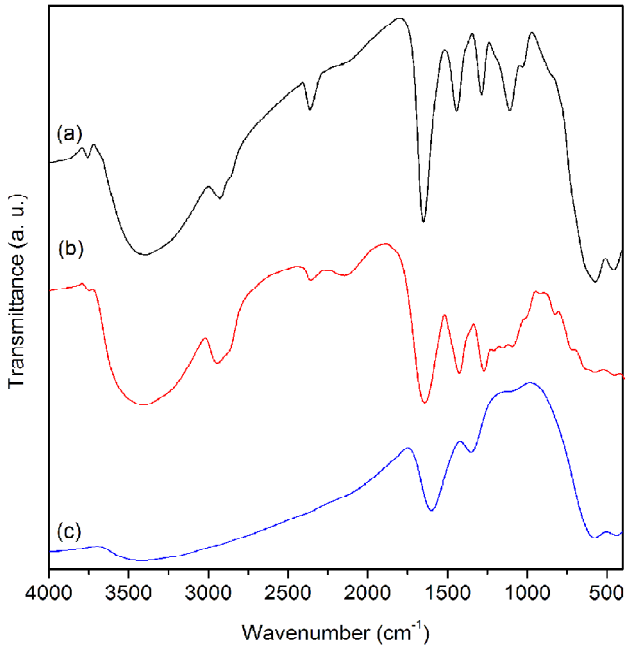

Fig. 9. IR spectra of the (a) PVP coated γ-Fe_2O_3, (b) pure PVP and (c) uncoated γ-Fe_2O_3 samples.

file intensity in the Raman spectra[30]. This very often changes or destroys composition of the material or transforms it into a different chemical phase. Grasset *et al.* have reported that the intensity of the typical Raman vibrations of γ-Fe_2O_3 decreases and gradually vanishes with increasing laser power and finally Raman peaks for hematite phase become stronger under laser power of 15 mW[30]. Therefore, in the present study, it is believed that both the maghemite samples are transformed into the α-Fe_2O_3 phase under the laser power of 20 mW.

IR spectroscopy:

The IR spectrum of pure PVP shows several characteristic bands, particularly at 2958, 2858 cm^{-1} and in the fingerprint region (1499, 1467, 1430 and 1287 cm^{-1}). The PVP coated γ-Fe_2O_3 exhibits the typical peaks arising from PVP residue which indicates the successful attachment of PVP macromolecules to the surface of nanoparticles. Both the oxide samples display two peaks in the wave number range of 580–440 cm^{-1} which can be attributed to Fe-O vibration in Fe_2O_3[31]. Literature suggests that Fe_3O_4 generally exhibits a single band around 590 cm^{-1} for typical Fe-O vibrations[25,32]. The absence of this particular band (590 cm^{-1}) in the IR spectra of both the synthesized iron oxide samples suggests that Fe_3O_4 phase is absent. Furthermore, the color of both the synthesized materials is red-brown which is significantly different from that of black magnetite.

Optical properties:

The UV-Vis absorption spectrum of the α-Fe_2O_3 sample obtained after 4 h solvothermal aging of 1 g of the ferrous isonicotinate tetrahydrate is shown in Fig. 10. It exhibits two prominent absorption features at 391 and 472 nm as parts of the absorption envelope ranging from ~200 nm to ~740 nm. Literature suggests that the iron oxides generally show three types of optical transitions: the ligand to metal charge-transfer transitions (LMCT), the ligand field transitions (d-d transitions) and the pair excitations[33]. In our case, the band around 391 nm may be attributed to the LMCT transition and partly to the Fe^{3+} ligand field transition [$^6A_1 \rightarrow {}^4E$ (^4G)][26]. On the other hand, the band around 472 nm can be assigned to the $^6A_1 \rightarrow {}^4E$, $^4A_1$ (^4G) ligand field transitions of Fe^{3+} [34]. It has been reported that the LMCT transitions in the wavelength range of 200–400 nm usually dominate the optical properties of nanoparticles and nanorods[34]. Fan *et al.* reported that nanotubes with an average diameter of 98 nm and average

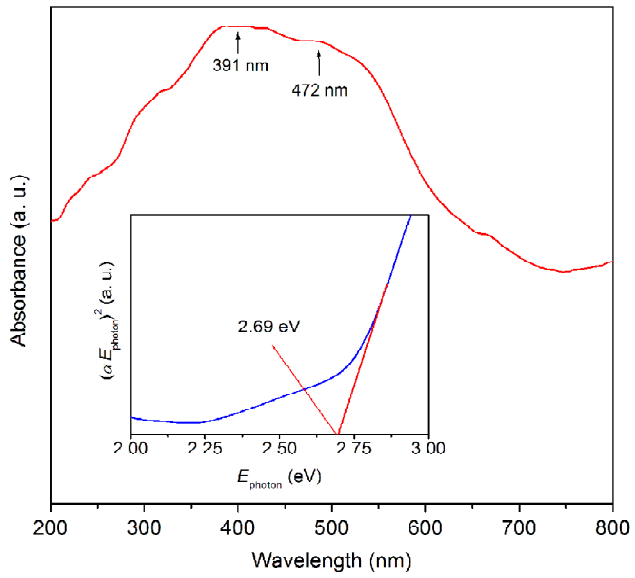

Fig. 10. UV-Vis diffuse reflectance spectrum of the α-Fe_2O_3 sample obtained via 4 h solvothermal aging of 1 g of ferrous isonicotinate tetrahydrate. Inset is the representative plots of (α E_{photon}) 2 versus E_{photon} for the direct transition.

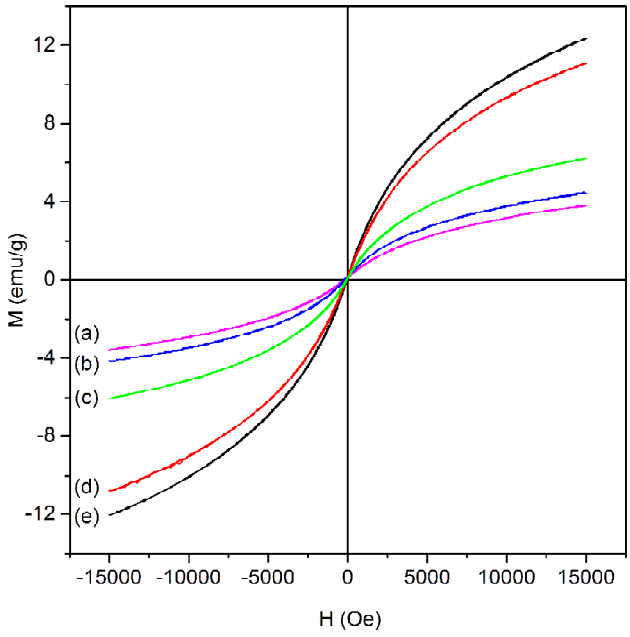

Fig. 11. Room temperature M-H curves of the as-synthesised α-Fe_2O_3 samples obtained after (a) 4 h, (b) 2 h solvothermal aging of 0.5 g of the ferrous isonicotinate tetrahydrate, and after (c) 20 h, (d) 4 h and (e) 2 h aging of 1 g of the ferrous isonicotinate tetrahydarte.

length of 260 nm showed two absorptions at the 450 nm and 550 nm[35]. The band gap energy is estimated following the classical Tauc's relationship[36]. It has been reported that n = 1/2 (allowed direct transition) gives the best description for the energy structure of the semiconductor materials. The calculated band gap energy (2.69 eV) is quite large compared to that of the bulk hematite (2.1 eV). The observed band gap expansion is caused by the quantum size effect[37].

Magnetic properties:

The room temperature M-H curves of the α-Fe_2O_3 samples are presented in Fig. 11. All of the materials exhibit unsaturated magnetization even at the maximum applied field. Moreover, the absence of coercive force and remanence magnetization indicates the typical superparamagnetic behavior[17,38]. Superparamagnetic properties of the α-Fe_2O_3 have also been observed in many instances by different research groups. Tang *et al.* have reported the supermagnetic behavior of α-Fe_2O_3 nanorods with diameter of 15–25 nm and lengths up to 170–300 nm[17]. On the other hand, Mørup *et al.* reported the superparamagnetic behavior of spherical α-Fe_2O_3 nanoparticles with diameter about 16 nm[39].

Both the maghemite samples discussed in the present work display typical hysteresis loops (Fig.10). The observed saturation magnetization (M_s = 38 emu/g) of the uncoated iron oxide is lower than that of bulk γ-Fe_2O_3 (74 emu/g)[22] which may be attributed to crystal and shape anisotropy[40]. The measured remanence magnetization (M_r = 2.8 emu/g) and coercivity (H_c = 36 Oe) are larger than those expected on the basis of the reduced particle size. This may be caused by extensive agglomeration of the magnetic particles[41]. Thus, the synthesized oxide shows ferromagnetic character. The average particle size (9 nm) of the uncoated γ-Fe_2O_3 sample lies within the range of critical size (around 20 nm) of a single magnetic domain[42]. The superparamagnetic properties of cubic and spherical maghemite nanoparticles of similar sizes (~14 nm) were experimentally and theoretically studied by Salazar-Alvarez *et al.*[43].

In the narrow applied filed-range (–1.5 T to 1.5 T), magnetization of the PVP coated γ-Fe_2O_3 sample appears to be almost unsaturated. The measured remanent magnetization (M_r = 0.50 emu/g) and coercivity ((H_c = 5.0 Oe) values are quite low. The observed decrease in coercivity compared to that of the uncoated γ-Fe_2O_3 can be attributed to the decrease in particle size and agglomeartion[41].

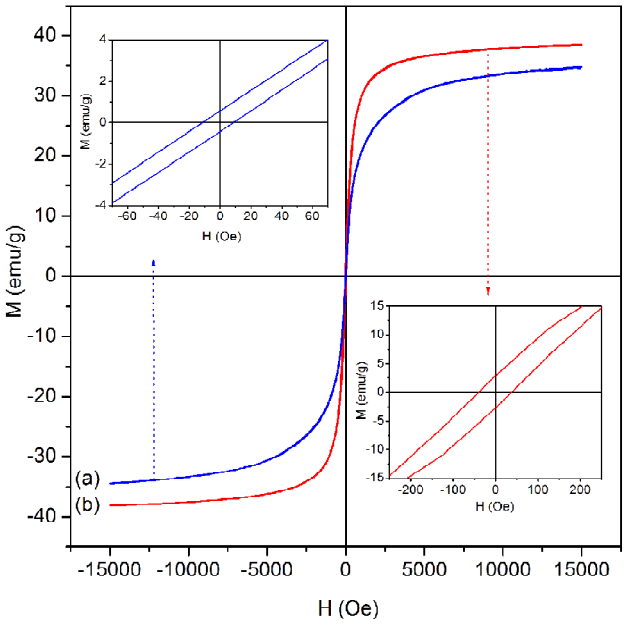

Fig. 12. Room temperature magnetic hysteresis loops of the as-synthesised (a) PVP coated γ-Fe_2O_3 and (b) γ-Fe_2O_3. Insets show their corresponding low field loops.

Table 1. TBHP oxidation of styrene catalyzed by Fe_2O_3 nanomaterials

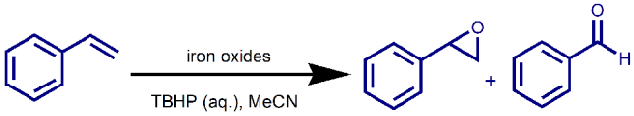

Catalysts	Styrene conversion[a] (%)	Styrene oxide[a] (%)	Co-products[a] (%)
α-Fe_2O_3 (aging 1 h)	27.3	51.8	48.2
α-Fe_2O_3 (aging 2 h)	56.3	75.9	24.1
α-Fe_2O_3 (aging 4 h)	83.3	89.7	11.3
α-Fe_2O_3 (aging 20 h)	89.3	76.7	23.3
γ-Fe_2O_3	73.8	75.1	24.9
PVP coated γ-Fe_2O_3	77.5	80.9	20.1

Reaction condition: substrate, 5 mmol; catalyst amount, 10 mg; solvent, MeCN (5 mL); TBHP (70% aq.) amount, 2 mL (14 mmol); temperature, 70°C; reaction time 5 h. [a]Obtained from GC analysis.

Catalysis of styrene oxidation:

As detailed in the experimental section, the catalytic activities of the iron oxide nanomaterials synthesized by us via precursor method have been tested in the liquid phase oxidation of styrene using aqueous TBHP as the oxidant under heterogeneous condition. Table 1 shows the results on our studies on the oxidation of styrene.

It is found that the styrene conversion increases gradually with reaction time and after 5 h of reaction, it reaches 89% with ~76% selectivity for styrene epoxide over α-Fe_2O_3 catalyst. The table shows that the conversion of styrene into its styrene oxide (SO) increases from 27% to 89%, as the catalyst α-Fe_2O_3 (aging time, 1 h) is replaced by α-Fe_2O_3 (aging time, 20 h). Since it has been shown above that the prolonged solvothermal aging enhances the crystallinity of the oxide materials, the conversionof styrene may perhaps be correlated to the degree of crystallinity of α-Fe_2O_3 catalysts.

In other words, prolonged aging gives more crystalline α-Fe_2O_3 catalysts which in turn give greater styrene conversion. Although, the styrene conversion is found to gradually increase with solvothermal aging (or crystallinity) of the catalysts, the selectivity for SO (the epoxide) does not increase in a regular manner with the increasing aging of the catalysts. The data presented in the table suggest that the selectivity for the epoxide product increases with the catalyst-aging time and reaches a maximum value of ~90% over α-Fe_2O_3 (aging time, 4 h) and then declines to ~77% over α-Fe_2O_3 (aging time, 20 h). When the reaction is carried out without any catalyst, a very poor styrene conversion is observed which proves the catalytic effectiveness of α-Fe_2O_3 for the styrene oxidation reaction. Additionally, a reaction carried out under analogous conditions with commercially available hematite powder gave only 20% conversion with 44% selectivity for epoxidation. Furthermore, benzal-dehyde and a trace amount of benzoic acid have been detected as the other products in the reactions catalyzed by both the bulk and nanosized hematite.

However, styrene conversion increases from 73.8% to 77.5% upon replacing the bare γ-Fe_2O_3 by coated γ-Fe_2O_3 catalyst leading to rise in epoxide selectivity from 75.1% to 80.9%. This indicates that while α-Fe_2O_3 is a better catalyst than γ-Fe_2O_3, among the two forms of γ-Fe_2O_3 nanocatalysts the PVP-coated form is marginally more active and selective for epoxidation. It is clear from the present results that both α-Fe_2O_3 and γ-Fe_2O_3 synthesized by us by making use of ferrous isonicotinate tetrahydrate as the precursor show higher styrene conversion as well as epoxide selectivity compared to other literature examples in which iron oxides have

been used as the catalysts in the oxidation of styrene[10–12].

Earlier, 43% styrene conversion with 74% epoxide selectivity along with benzaldehyde as the side-product was reported by Huang *et al.* in the epoxidation of styrene with TBHP over porous Fe_3O_4 nanoparticles under heterogeneous condition[10]. They could obtain an enhanced styrene conversion only upon the immobilization of Au nanoparticles on their Fe_3O_4 nanocatalyst. Liang *et al.* reported that only 4% styrene conversion with 22% epoxide selectivity could be observed over nanoscale Fe_2O_3 catalyst using O_2 as the oxidant[11]. Complete conversion of styrene with 84% epoxide selectivity was reported after 13 h of the reaction using TBHP over nanostructured Fe_3O_4 having deposited Ag nanoparticles[12]. The iron oxide nanoshell catalysts reported by Rak *et al.*[44] are more efficient with up to 90% styrene conversion and 73% product selectivity. In this case, however, the preferred product is benzaldehyde which forms with the concomitant loss of one carbon atom per molecule styrene molecule, thus releasing a molecule of one molecule of CO_2 via an oxidative cleavage of the C=C bond. In our previously published work on the use of a differently prepared α-Fe_2O_3 nanocatalyst, 78% styrene conversion with 66% selectivity for epoxide with TBHP as oxidant after 8 h of reaction was reported[13]. The styrene conversion and epoxide selectivity achieved, and the short reaction time and reaction temperature required for achieving high product yield and selectivity suggest that both hematite and maghemite nanocatalysts prepared by us are highly efficient as catalysts in the liquid phase oxidation of styrene with aq. TBHP as the oxidant.The formation of the epoxide as the preferred product is also a significant finding because styrene oxide is an important synthetic intermediate that can be subsequently converted to many valuable chemical products[45].

A few experiments to examine the recyclability of the catalysts have also been performed. In doing so, samples of the two oxide nanocatalysts displaying the best catalytic activities have been chosen. The iron oxide catalysts were removed from the reaction mixture by means of an external magnet and then the same were dried at 60°C for about 4 h and reused. Catalytic efficiencies of the dried catalysts were then examined under identical reaction conditions. Both the styrene conversion and selectivity for epoxide product remained unaltered for the catalyst α-Fe_2O_3 (aging time, 4 h) and the efficiency remained almost unaltered even after three successive reuses. However, styrene conversion and epoxide selectivity for the PVP coated γ-Fe_2O_3 gradually dropped to 70% and 75% respectively. With more detailed further studies, the present findings should prove valuable because the catalysts synthesized by us work without requiring the use of a noble metal, are nontoxic, inexpensive and easy to prepare and also because the heterogeneous catalysts being magnetic, they are easy to separate from the reaction mixture at the end of the reaction.

Conclusions

Nanometer-sized α-Fe_2O_3 (hematite) and γ-Fe_2O_3 (maghemite) particles have been succesfully prepared using ferrous isonicotinate tetrahydrate as a single molecular precursor. While hematite nanorods are syntheised via a facile solvothermal route with an excellent control over the rod-like morphology of the particles, spherical maghemite nanoparticles are obtained via thermal treatment of the iron complex under atmospheric pressure. The duration of solvothermal aging influences the crystallinity as well as size of α-Fe_2O_3 nanocrystals. On the other hand, lowering of precursor concentration improves the crystallinity of α-Fe_2O_3 nanorods. The γ-Fe_2O_3 particles appear to be agglomerated in the absence of PVP during synthesis, but these are obtainable in a highly dispersed state via PVP coating. Magnetic studies suggest the suparparamagnetic behavior of α-Fe_2O_3 as well as PVP coated γ-Fe_2O_3 samples and ferromagnetic behavior of the uncoated γ-Fe_2O_3. The synthesized iron oxides are found to be very effective as catalysts in the epoxidation of styrene using TBHP under heterogeneous condition.

Acknowledgements

Financial support from CSIR, New Delhi (Sanction No. 01(2404)/10/EMR-II) is gratefully acknowledged. RAB thanks CSIR and ZI and AT thank UGC (India) for Research Fellowships. We thank DST-SAIF, Gauhati University (Guwahati) and NEHU (Shillong) for XRD and electron microscopic data respectively and IIT Guwahati for magnetic data. We also thank CMC, NCL (Pune) for providing us the Raman spectroscopic data.

References

1. B. K. Das, S. J. Bora, M. Chakrabortty, L. Kalita, R. Chakrabarty and R. K. Barman, *J. Chem. Sci.*, 2006, **118**, 487.
2. B. K. Das, S. J. Bora and M. Chakrabortty, *J. Indian Chem. Soc.*, 2019, **96**, 317.

3. A. Gaur, N. N. Nair, B. D.Shrivastava, B. K. Das, M. Chakrabortty, S. N. Jha and D. Bhattacharyya, *Chem. Phys. Lett.*, 2018, **692**, 382.
4. M. Chakrabortty, J. N. Ganguli, S. J. Bora and B. K. Das, *Indian J. Chem.*, 2010, **49A**, 876.
5. A. Talukdar, R. A. Bepari, S. Nath, B. K. Das and M. Chakrabortty, *J. Assam Sc. Soc.*, 2018, **59**, 109.
6. R. A. Bepari, M. Chakrabortty, S. J. Bora and B. K. Das, *Ind. J. Chem.*, 2014, **53A**, 1344.
7. C. Ruxin, W. Shuo and Y. Bing, *Adv. Mater. Res.*, 2011, **148**, 1124.
8. G. M. Bhalerao, A. K. Sinha and A. K. Srivastava, *J. Nanosci. Nanotech.*, 2009, **9**, 5502.
9. S. Zhao, H. Y. Wu, L. Song, O. Tegus and S. Asuha, *J. Mater. Sci.*, 2009, **44**, 926.
10. C. Huang, H. Zhang, Z. Sun, Y. Zhao, S. Chen, R. Tao and Z. Liu, *J. Colloid Interf. Sci.*, 2011, **364**, 298.
11. J. Liang, Q. Tang, G. Meng, H. Wu, Q. Zhang and Y. Wan, *Chem. Lett.*, 2004, **33**,1140.
12. D. H. Zhang, G. D. Li, J. X. Lia and J. H. Chen, *Chem. Commun.*, 2008, 3414.
13. R. A. Bepari, P. Bharali and B. K. Das, *Saudi J. Chem.*, 2017, **21**, S170.
14. A. Pathak and P. Pramanik, *PINSA*, 2001, **67A**, 47.
15. L. Chen, X. Yang, J. Chen, J. Liu, H. Wu, H. Zhan, C. Liang and M. Wu, *Inorg. Chem.*, 2010, **49**, 8411.
16. X. G. Peng, L. Manna, W. D. Yang, J. Wickham, E. Scher, A. Kadavanich and A. P. Alivisatos, 2010, **49**, 8411.
17. B. Tang, G. Wang, L. Zhuo, J. Ge and L. Cui, *Inorg. Chem.*, 2006, **45**, 5196.
18. Y. Wenyan, C. Xing, C. Minghua, H. Changwen and W. Bingqing, *J. Phys. Chem.*, 2009, **C 113**, 15897.
19. T. P. Almeida, M. W. Fay, Y. Zhu and P. D. Brown, *Nanoscale*, 2010, **2**, 2390.
20. M. Zhu and G. Diao, *J. Phys. Chem.*, 2011, **C115**, 18923.
21. T. Hyeon, S. S. Lee, J. Park, Y. Chung and H. B. Na, *J. Am. Chem. Soc.*, 2001, **123**, 12798.
22. N. S. Chaudhari,S. S. Warule, S. Muduli, B. B.Kale, S. Jouen, B. Lefez, B. Hannoyer and S. B. Ogale, *Dalton Trans.*, 2011, **40**, 8003.
23. Q. Han, Z. Liu, Y. Xu, Z. Chen, T. Wang and H. Zhang, *J. Phys. Chem.*, 2007, **C111**, 5034.
24. H. M. Fan, G. J. You, Y. Li, Z. Zheng, H. R. Tan, Z. X. Shen, S. H. Tang and Y. P. Feng, *J. Phys. Chem.*, 2009, **C113**, 9928.
25. S. Xuan, F. Wang, Y.-X. J. Wang, J. C. Yu and K. C.-F. Leung, *Langmuir*, 2009, **25**, 11835.
26. D. Bersani, P. P. Lottici and A. Montenero, *J. Raman Spectrosc.*, 1999, **30**, 355.
27. D. Bersani, P. P. Lottici and X.-Z. Ding, *Appl. Phys. Lett.*, 1998, **72**, 73.
28. O. N. Shebanova and P. Lazor, *J. Solid State Chem.*, 2003, **174**, 424.
29. R. M. Cornell and U. Schwertmann, "The Iron Oxides", 2nd ed., Wiley-VCH, Germany, 1996.
30. Y. E. Mendili, J.-F. Bardeau, N. Randrianantoandro, A. Gourbil, J.-M.Greneche, A.-M. Mercier and F. Grassetc, *J. Raman Spectrosc.*, 2011, **42**, 239.
31. N. Du, Y. Xu, H. Zhang, C. Zhai and D. Yang, *Lett.*, 2010, **5**, 1295.
32. L. Kong, X. Lu, X. Bian, W. Zhang and C. Wang, *ACS Appl. Mater.*, *Interfaces*, 2011, **3**, 35.
33. Y. P. He, Y. M. Miao, C. R. Li, S. Q. Wang, L. Cao, S. S. Xie, G. Z. Yang, B. S. Zou and C. Burda, *Phys. Rev.*, 2005, **B71**, 125411.
34. L. Jiabiao, D. Xiaochuan, M. Jianmin, P. Peng, K. Tongil and Z. Wenjun, *ACS Nano*, 2009, **3**, 3749.
35. H. M. Fan, G. J. You, Y. Li, Z. Zheng, H. R.Tan, Z. X. Shen, S. H. Tang and Y. P. Feng, *J. Phys. Chem.*, 2009, **C113**, 9928.
36. S. Tsunekawa, T. Fukuda and A. Kasuya, *J. Appl. Phys.*, 2000, **87**, 1318.
37. C. Q. Sun, B. K. Tay, S. Li, X. W. Sun, S. P. Lau and T. P. Chen, *Mater. Phys. Mech.*, 2001, **4**, 129.
38. C. P. Bean and J. D. Livingston, *J. Appl. Phys.*, 1959, **30**, S120.
39. F. Bødker, M. F. Hansen, C. B. Koch, K. Lefmann and S. Mørup, *Phys. Rev.*, 2000, **B61**, 6826.
40. D. E. Zhang, X. J. Zhang, X. M. Ni, J. M. Song and H. G. Zheng, *Cryst. Growth Des.*, 2007, **7**, 2117.
41. Y. Zhu, W. Zhao, H. Chen and J. Shi, *J. Phys. Chem.*, 2007, **C111**, 5281.
42. R. E. Dunin-Borkowski, M. R. McCartney, R. B. Frankel, D. A. Bazylinski, M. Posfai and P. R. Buseck, *Science*, 1998, **282**, 1868.
43. G. Salazar-Alvarez, J. Qin, V. Sepelak, I. Bergmann, M. Vasilakaki, K. N. Trohidou, J. D. Ardisson, W. A. A. Macedo, M. Mikhaylova, M. Muhammed, M. D. Baro and J. Nogues, *J. Am. Chem. Soc.*, 2008, **130**, 13234.
44. M. J. Rak, M. Lerro and A. Moores. *Chem. Commun.*, 2014, **50**, 12482.
45. M. S. Batra, R. Dwivedi and R. Prasad, *ChemistrySelect*, 2019, **4**, 11636.